

Shortcut to adiabaticity in spinor condensates

Arnau Sala,^{1,*} David López Núñez,¹ Joan Martorell,¹ Luigi De Sarlo,^{2,†} Tilman Zibold,^{2,‡} Fabrice Gerbier,² Artur Polls,^{1,3} and Bruno Juliá-Díaz^{1,3,4}

¹*Departament de Física Quàntica i Astrofísica, Facultat de Física, Universitat de Barcelona, E-08028 Barcelona, Spain*

²*Laboratoire Kastler Brossel, Collège de France, CNRS, ENS-PSL Research University, UPMC-Sorbonne Universités, 11 place Marcelin Berthelot, 75005 Paris, France*

³*Institut de Ciències del Cosmos, Universitat de Barcelona, ICC-UB, Martí i Franquès 1, E-08028 Barcelona, Spain*

⁴*ICFO-Institut de Ciències Fotòniques, The Barcelona Institute of Science and Technology, 08860 Castelldefels, Spain*

(Received 14 July 2016; published 12 October 2016)

We devise a method to shortcut the adiabatic evolution of a spin-1 Bose gas with an external magnetic field as the control parameter. An initial many-body state with almost all bosons populating the Zeeman sublevel $m = 0$ is evolved to a final state very close to a macroscopic spin-singlet condensate, a fragmented state with three macroscopically occupied Zeeman states. The shortcut protocol, obtained by an approximate mapping to a harmonic oscillator Hamiltonian, is compared to linear and exponential variations of the control parameter. We find a dramatic speedup of the dynamics when using the shortcut protocol.

DOI: [10.1103/PhysRevA.94.043623](https://doi.org/10.1103/PhysRevA.94.043623)

I. INTRODUCTION

Ultracold spinor Bose gases provide a beautiful example to study fragmented Bose-Einstein condensates (BECs) [1], where Bose-Einstein condensation occurs in two or more single-particle states simultaneously. This is an unusual scenario, in contrast with conventional Bose-Einstein condensation, where bosons cluster together into a single state. For single-component bosons, condensation in a single state is enforced by repulsive interactions: The energetic cost of fragmentation is too high because of the associated exchange energy [2].

For bosons with an internal degree of freedom, one can escape this mechanism by building correlations between the particles to cancel the exchange energy [1]. A spin-1 BEC with antiferromagnetic interactions in a tight trap has been predicted to host such fragmented condensates for vanishing magnetic fields [3–10]. The atoms condense into a single spatial mode but there remains a large internal degeneracy at the single-particle level. Antiferromagnetic interactions lift this degeneracy and lead to a total spin-singlet ground state which is completely fragmented between the three sublevels. The many-body singlet state displays strong quantum correlations and has attracted much theoretical interest. Its experimental realization would enable us to investigate the phenomenon of condensate fragmentation due to symmetry (here spin rotational symmetry) in boson systems, a fundamental issue in quantum gases [1].

This spin-singlet fragmented condensate is fragile against any perturbation lifting the single-particle degeneracy, such as external magnetic fields [4–6]. In experiments with alkali atoms, the most relevant perturbation is the quadratic Zeeman

splitting between the Zeeman sublevels $m = 0$ and $m = \pm 1$ [11]. For a finite atom number N , there is a small but nonvanishing window where the singlet state survives as the quadratic Zeeman splitting increases from 0, before a crossover to a single $m = 0$ condensate takes place (“single-BEC domain”) [8–10]. An appropriate witness of the transition is the variance $\Delta N_0 \equiv \sqrt{\langle N_0^2 \rangle - \langle N_0 \rangle^2}$, which goes from $\propto N$ in the spin-singlet state to $\propto \sqrt{N}$ in an uncorrelated many-body state [10].

Because of the sensitivity to external perturbations, the singlet state has so far eluded experimental observation. The gap to the first excited state is smaller than the typical interaction energy by a factor that scales as the inverse of the number of atoms [3]. Evaporative cooling used to produce quantum gases is unable to reach such ultralow temperatures. Another procedure is to adiabatically produce the singlet state by first applying a magnetic field and condensing in the $m = 0$ state and then slowly removing the field to produce the desired singlet state (see the sketch in Fig. 1). In order to stay adiabatic, the dynamics must be very slow in view of the small energy scales involved, making the procedure vulnerable to heating or inelastic losses.

In this article we introduce a way to shortcut the adiabatic following and thus produce the desired final state in times much shorter than those needed in adiabatic processes. Such methods have recently been derived for a number of quantum mechanical systems (see, for instance, Ref. [12]) and promise to provide important advances in actual implementations of quantum technologies, for instance, trapped ions [13]. Exact protocols have been derived for particular problems, e.g., the quantum harmonic oscillator [14]. In other cases, approximate procedures, obtained by adapting exact ones, have been proven to be quite promising when applied to quantum many-body systems [15–17].

As will be shown, the approximate shortcut protocol is obtained from a large- N limit of the quantum many-body system. This limit allows us to map our original many-spin problem into an effective harmonic oscillator, for which an exact solution is available [14]. Interestingly, very recently a similar harmonic description of a spinor BEC has allowed

*Present address: Department of Physics, Norwegian University of Science and Technology, NO-7491 Trondheim, Norway.

†Present address: SYRTE, Observatoire de Paris, LNE, CNRS, UPMC, 61 avenue de l’Observatoire, 75014 Paris, France.

‡Present address: Department of Physics, University of Basel, Klingelbergstrasse 82, 4056 Basel, Switzerland.

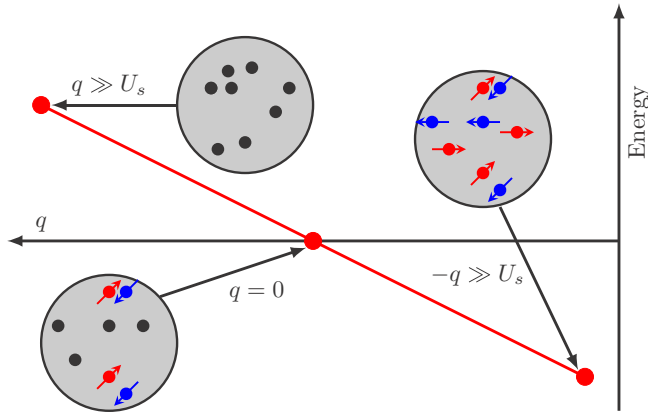


FIG. 1. Sketch of the proposed experimental protocol. A spin-1 BEC is prepared at large positive values of the quadratic Zeeman energy (QZE) q with all atoms in the $m = 0$ state. In this regime, the initial state is very close to the ground state (arbitrarily close as $q \rightarrow \infty$). In the adiabatic method, the QZE is slowly reduced in such a way that the state of the system always remains close to the instantaneous ground state. Stopping the QZE ramp at $q = 0$, the system ends up in a total spin-singlet ground state with strong spin correlations. Stopping the ramp at a large, negative value of q , we prepare instead a twin Fock state with half the atoms in the Zeeman states $m = \pm 1$. In this paper we target the production of the singlet state and examine this procedure and alternative ramps which are not adiabatic but result in a state close to the ground state in a much shorter time.

the authors in Ref. [18] to prove parametric amplification of a spinor system. This work proves experimentally the appropriateness of the harmonic description.

The article is organized as follows. In Sec. II, we present the theoretical model to describe the spinor BEC and discuss the adiabatic preparation of the ground state. In Sec. III we obtain our protocol to shortcut the adiabatic evolution in the spinor system from a continuum approximation to the spin dynamics. In Sec. IV we apply our shortcut protocol to the BEC regime (dominated by the quadratic Zeeman energy). In Sec. V we consider a broader range of parameters, discussing the quality of our protocol to produce fragmented BECs starting from the BEC side. In Sec. VI we present results making use of current experimental setups [18]. In Sec. VII, we briefly summarize our work and present the main conclusions.

II. THEORETICAL MODEL

A. Description of the system

We consider an ultracold gas of spin-1 bosons in a harmonic trap under the action of an external magnetic field. We assume a single spatial mode in the trap, that is, all bosons condense in the same spatial orbital irrespective of their internal state. With this assumption we are left with three single-particle states, $|+1\rangle$, $|0\rangle$, and $|-1\rangle$, corresponding to the Zeeman states with magnetic quantum numbers $m = +1, 0$, and -1 , respectively. The linear Zeeman effect acts only as a shift in the energy and does not contribute to the determination of the equilibrium state. The main contribution of the magnetic field is the quadratic, or second-order, Zeeman effect (QZE) [11]

(see Appendix A). Under these assumptions, the system is well described by the Hamiltonian [8,9]

$$\hat{H} = \frac{U_s}{2N} \hat{S}^2 - q \hat{N}_0, \quad (1)$$

where $U_s > 0$ is the spin interaction energy per atom, N is the number of atoms, \hat{S}^2 is the (dimensionless) total spin operator, q is the quadratic Zeeman energy, and \hat{N}_m is the number operator of the Zeeman state $m = 0, \pm 1$.

The first term on the right-hand side of Eq. (1) describes antiferromagnetic interactions between pairs of atoms and favors configurations with a low total spin S . In the absence of the quadratic Zeeman term, $q = 0$, the eigenstates are known analytically and are given by the total spin eigenstates $|N, S, M\rangle$, where S is the total spin and M the eigenvalue of \hat{S}_z , the projection of the total spin on the z axis. This is the basis we use in the following sections. Low- S configurations are obtained by putting many spin-1 atoms to form spin-singlet pairs, while the remaining atoms can occupy any Zeeman sublevel. For practical convenience, from now on N is set to an even number. The ground state for even N is the total spin singlet $|N, S = 0, M = 0\rangle$. This highly fragmented state, termed the “spin-singlet condensate” (SSC), takes the form of a condensate of delocalized spin-singlet pairs,

$$|\text{SSC}\rangle \propto (\hat{A}^\dagger)^{N/2} |\text{vac}\rangle, \quad (2)$$

where $\hat{A}^\dagger = (\hat{a}_0^\dagger)^2 - 2\hat{a}_{+1}^\dagger \hat{a}_{-1}^\dagger$ creates a pair of atoms in the two-particle singlet state, \hat{a}_m is an annihilation operator for a particle in the Zeeman state with the third component of the angular momentum equal to m , and $|\text{vac}\rangle$ is the boson vacuum. This fragmented state is characterized by three macroscopically populated states, $\langle N_{+1} \rangle = \langle N_0 \rangle = \langle N_{-1} \rangle = N/3$, with large fluctuations of the individual components [1].

The second term in Eq. (1) describes the interaction of the system with the external magnetic field. In the noninteracting limit $U_s \rightarrow 0$ and for $q > 0$, the QZE forces all the spins to occupy the state $m = 0$, thus forming a single BEC with $\langle N_0 \rangle = N$ and $\langle N_{+1} \rangle = \langle N_{-1} \rangle = 0$, the so-called z -polar state:

$$|\text{Polar}\rangle_z \propto (\hat{a}_0^\dagger)^N |\text{vac}\rangle. \quad (3)$$

It is noteworthy that M remains fixed when q is changed, because the Hamiltonian commutes with \hat{S}_z . This is a good approximation to the behavior due to the experimental conditions of the atomic quantum gases, which are highly isolated from the environment, and to the microscopic rotational invariance of the spin exchange interaction [11].

For simplicity, we take $M = 0$. Also, as the number of particles N is fixed during the evolution, we omit it in the kets; thus, from now on we use the notation $|S\rangle \equiv |N, S, 0\rangle$.

B. Ground state for intermediate values of $|q|$

For generic values of q and U_s , we write a general state $|\phi\rangle$ with fixed N and $M = 0$ as $|\phi\rangle = \sum_S c_S |S\rangle$. The Schrödinger equation $\hat{H}|\phi\rangle = E|\phi\rangle$ in the S basis reduces to the following discrete eigenvalue equation (see Appendix B):

$$h_{S,S+2} c_{S+2} + h_{S,S-2} c_{S-2} + h_{S,S} c_S = E c_S. \quad (4)$$

In the upper panel in Fig. 2 we show the transition from the U_s -dominated fragmented regime to the single-BEC regime

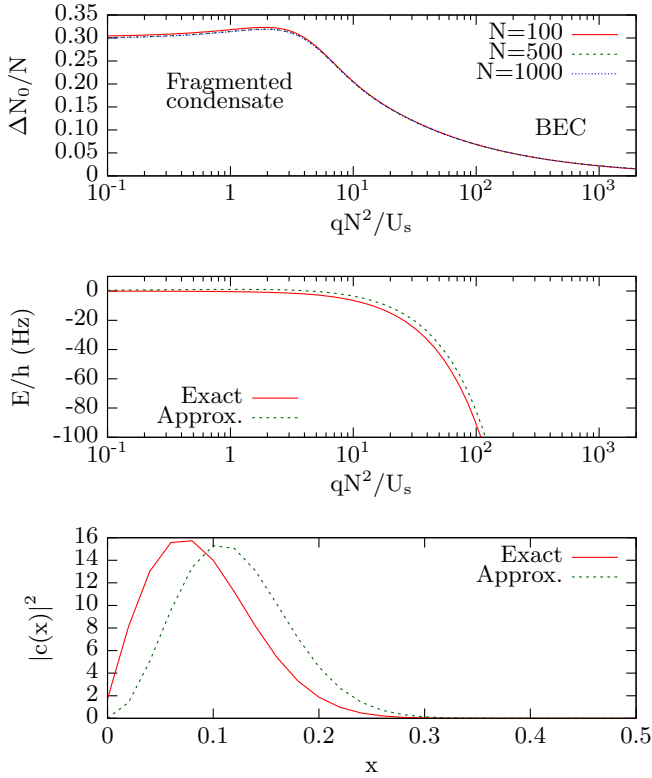


FIG. 2. Upper panel: Fluctuation of the number of particles in the $m = 0$ manifold, $\Delta N_0/N$, computed for three numbers of atoms. Middle panel: Energy of the ground state of the exact system compared with the energy of the ground state obtained in Eq. (10) for different values of the parameter q . When $qN^2U_s^{-1} < 2$, the system becomes U_s dominated, and thus, the energy is constant [see Eq. (10)]. It is noteworthy that in both the fragmented (U_s -dominated) and the BEC (q -dominated) regimes, the approximate value of the energy agrees well with the exact one. Lower panel: Wave function squared of the ground state compared to the value obtained with the continuous approximation described in the text. The middle and lower panels were obtained for a system of $N = 100$ spins. In all cases, $U_s/h = 104.13$ Hz. For the lower panel, we have used $q = U_s$.

when the ratio qN^2/U_s is varied. The transition between the two regimes takes place at values $qN^2U_s \simeq 1$ and is seen in the behavior of the variance $\Delta N_0/N$ of the populations in the $m = 0$ Zeeman state. As explained in Sec. I, in the uncorrelated BEC state, $\Delta N_0 \propto \sqrt{N}$, while in the spin-singlet state the fluctuations are much larger, $\Delta N_0 \propto N$.

C. Adiabatic preparation of the singlet ground state

Experimentally, the value of the QZE can be controlled easily in real time. For instance, for sodium atoms with hyperfine spin $F = 1$ in a magnetic field B , the quadratic Zeeman shift contributes a *positive* amount to q . It is also possible to achieve $q < 0$ by using the differential level shift induced in the individual Zeeman sublevels by a far off-resonant microwave field (see [19] for details). With a suitable choice of the microwave polarization, detuning, and power, the sign and magnitude of q can be changed at will.

This experimental control of the QZE opens a way to the generation of strongly correlated states in spin-1 quantum gases. The principle is the following. For zero magnetization and a large and positive QZE, the ground state is very close to a single BEC with all atoms in the $m = 0$ Zeeman state. A good approximation of this state can be prepared “by hand”, e.g., by applying radio-frequency pulses of a suitable frequency and polarization to a spin-polarized ensemble in $m = +1$, for instance. Starting from this initial state and slowly decreasing the value of q , the system will adiabatically follow its ground state and end up prepared in the SSC state given in Eq. (2) when $q \approx 0$.

We can estimate the speed at which the magnetic field should be decreased by the usual adiabatic criterion, $|\langle j|\dot{H}|i\rangle| \ll \hbar\omega_{ji}^2$, where $|i\rangle$ and $|j\rangle$ are two eigenstates of the Hamiltonian. The dangerous region is around $q < U_s/N^2$, where the energy gap to the first excited state takes its minimum value, $\sim 3U_s/N$. In this region, the QZE ramp has to be very slow. We make a crude estimate by assuming that q decreases between U_s and 0 in a time τ . Also in this region, $N_{\pm 1}$ are of the order of $N/3$. This leads to $|\langle j|\dot{H}|i\rangle| \sim NU_s/3\tau$ and to the adiabaticity criterion,

$$\tau \gg \frac{N^3\hbar}{27U_s}. \quad (5)$$

The catastrophic scaling $\tau \propto N^3$ shows that this method will be limited to small, mesoscopic samples. Using very long ramp times to fulfill the adiabaticity criterion will make the protocol vulnerable to experimental limitations not captured by the single-mode Hamiltonian, such as technical heating (specific for each experimental setup) and inelastic losses (specific for each atom).

Inelastic atom losses destroy the rotational symmetry since atoms are lost at random from any Zeeman state. A common source of inelastic losses is three-body recombination into a weakly bound molecule and a fast atom, resulting in three atoms lost from the trap. The total rate of these events can be written as $N\Gamma_3$, where $\Gamma_3 = (K_{3B}/N) \int d^3\mathbf{r} n(\mathbf{r})^3$ is determined by a species-dependent rate constant K_{3B} and by the spatial density n . Demanding less than one single inelastic event (on average) during the entire adiabatic protocol gives a bound $1/\tau \gtrsim N\Gamma_3$.

For illustrative purposes, we consider a gas of atoms condensing in the Gaussian ground state of a tight harmonic trap of frequency ω . The Gaussian ground state of the trap is a good approximation of the actual condensate wave function for a sufficiently low atom number $N < \sigma/\bar{a}$, with $\sigma = \sqrt{\hbar/m_A\omega}$ the harmonic oscillator length, with m_A the atomic mass, and with \bar{a} the spin-independent s -wave scattering length. The spin-dependent scattering length a_s is determined by the relation $U_s = (4\pi\hbar^2 a_s/m_A N) \int d^3\mathbf{r} n(\mathbf{r})^2$ [3]. The bound $1/\tau \gtrsim N\Gamma_3$ can be written as a bound on the maximum affordable atom number in the trap, written in compact form as

$$N \ll 5.1 \left(\frac{\sigma}{l_{3B}} \right)^{3/5}, \quad (6)$$

where $l_{3B} = (m_A K_{3B}/\hbar a_s)^{1/3}$ has the dimension of a length.

We specialize to the case of $F = 1$ sodium atoms, where $\bar{a} \approx 2.5$ nm and $a_s \approx 0.1$ nm [20] and the three-body loss rate

constant $K_{3B} \sim 1.6 \times 10^{-30}$ at $\cdot \text{cm}^6/\text{s}$ [21]. Using $\omega/(2\pi) = 2$ kHz, one finds $N \ll 36$ for the parameters given above, showing that the adiabatic approach is reserved for mesoscopic samples containing only a few atoms. This motivates us to find alternative solutions enabling a substantial speedup of the dynamics, which is our main objective in the rest of this paper.

III. SHORTCUTS TO ADIABATICITY

In view of the limitations of the adiabatic approach described above, we now examine a different method where the same final result can be reached in a much shorter time. In the literature, there are well-established shortcut protocols for one-body harmonic potentials [14]. Our strategy is to use these results to manipulate the many-spin system of interest by mapping it to an effective harmonic oscillator problem. We show in this section how a reasonable harmonic approximation to the many-body problem can be derived. By means of this approximate equation we map the shortcut protocol to the exact time-dependent Schrödinger equation built from Eq. (4).

A. Continuum approximation

The first step consists in deriving a continuum approximation to the Hamiltonian, Eq. (4). For large N and considering $1 \ll S \ll N$, the coefficients c_S can be assumed to vary smoothly from S to $S \pm 2$. Hence, c_S can be approximated by a continuous function $c(x)$, where $x \equiv S/N$ varies from 0 to 1. Following the derivations in Appendix C, we arrive at an effective Schrödinger-like equation for a harmonic oscillator

$$-\frac{\hbar^2}{2M^*}c''(x) + \frac{M^*\omega^2}{2}x^2c(x) = (E + Nq)c(x), \quad (7)$$

with the oscillator frequency given by $\hbar\omega = \sqrt{q(q + 2U_s)}$ and the oscillator “mass” by $M^*/\hbar^2 = N/2q$. The ground state obeying the boundary condition $c(0) = 0$ is the wave function

$$c(x) = \frac{2\sqrt{2}}{(\pi\sigma^2)^{1/4}} \frac{x}{\sigma} \exp\left(-\frac{x^2}{2\sigma^2}\right), \quad (8)$$

$$\sigma = \sqrt{\frac{2}{N}} \left(\frac{q}{q + 2U_s}\right)^{1/4}, \quad (9)$$

with energy

$$E = \frac{3}{2}\sqrt{q(q + 2U_s)} - Nq. \quad (10)$$

In Fig. 2 we compare the approximated and the exact solutions of our Hamiltonian. In the middle panel in Fig. 2 we see that the energy of the ground state is well reproduced by the harmonic approximation. In particular, it is interesting to note that the harmonic approximation works well both in the U_s -dominated regime and in the q -dominated one. Comparing the actual wave functions in the lower panel in Fig. 2, we can see that the solution of the approximate Hamiltonian has a shape similar to that of the exact wave function, although its maximum is slightly displaced towards higher values of S/N .

B. Shortcut protocol to adiabatic evolution

The idea behind the shortcut to adiabaticity in the time-dependent evolution of an harmonic oscillator is the following.

First, we consider that the system is initially in the ground state for a certain initial value $q(0)$ of the control parameter. Then we impose that at a given time t_f the system must be exactly in the ground state for a different value of the control parameter, $q(t_f) = q_f$. The goal is, thus, to find a function $q(t)$ that does the job. If the final time is sufficiently large, then any smooth ramp of the control parameter should work, since the evolution would be adiabatic. For short ramp times, an arbitrary ramp function would in general result in the excitation of many modes besides the ground state at the final time. The goal is therefore to engineer the ramp function in such a way as to minimize the excitations at $t = t_f$ and beyond; i.e., one seeks to produce an almost-stationary state once the ramp is completed.

The Schrödinger-like equation in Eq. (7) is already close to the one corresponding to a harmonic oscillator. The control parameter is the QZE, $q = q(t)$. The term on the right-hand side (a shift in the total energy) does not have any effect on the dynamics. We also limit ourselves to the regime $q \ll U_s$. The final Schrödinger-like equation, Eq. (7), is that of a harmonic oscillator with time-dependent “mass” and frequency $\omega^2(t) = 2q(t)U_s/\hbar^2$. A similar equation was considered in Ref. [16] to describe the dynamics of a two-mode Bose-Hubbard model. Following the same method, we look for a self-similar solution $c(x) = c_0(x/\rho)/\sqrt{n}e^{i\Theta(\rho, \dot{\rho})}$, with a scaling parameter ρ . Such a solution exists if the scaling parameter obeys the so-called Ermakov equation [14],

$$\ddot{\rho} + \omega(t)^2\rho = \frac{\omega_0^2}{\rho^3}. \quad (11)$$

The constant ω_0 is just an integration constant that we set to $\omega_0 = \frac{1}{\hbar}\sqrt{2q_0U_s}$. This, together with the substitution $b = 1/\rho$, gives

$$\frac{2\dot{b}^2}{b} - \ddot{b} + \frac{2q(t)U_s}{\hbar^2}b = \frac{2q_0U_s}{\hbar^2}b^5. \quad (12)$$

$b(t)$ is an arbitrary function that only has to satisfy the frictionless conditions

$$b_i \equiv b(t_0) = 1,$$

$$b_f \equiv b(t_f) = \left(\frac{q_f}{q_0}\right)^{1/4},$$

$$\dot{b}(t_0) = \dot{b}(t_f) = \ddot{b}(t_0) = \ddot{b}(t_f) = 0,$$

where t_0 will always be 0. There is an infinite set of functions $b(t)$ that can be used for this purpose, as the boundary conditions provide ample freedom to choose $b(t)$. Here we use a simple polynomial ansatz, taken from Ref. [14],

$$b(t) = b_i + 10(b_f - b_i)s^3 - 15(b_f - b_i)s^4 + 6(b_f - b_i)s^5, \quad (13)$$

where $s = t/t_f$. Thus, the function $q(t)$ is

$$q(t) = \left(2q_0U_s b^4 + \hbar^2 \frac{\ddot{b}}{b} - 2\hbar^2 \frac{\dot{b}^2}{b^2}\right) \frac{1}{2U_s}. \quad (14)$$

The six frictionless conditions previously mentioned uniquely determine the fifth-order polynomial chosen. We have tested that using a sixth-order polynomial or power-law functions did not improve the results, hence Eq. (13) is used in the rest of this work. Let us remark that the freedom in choosing $b(t)$ can

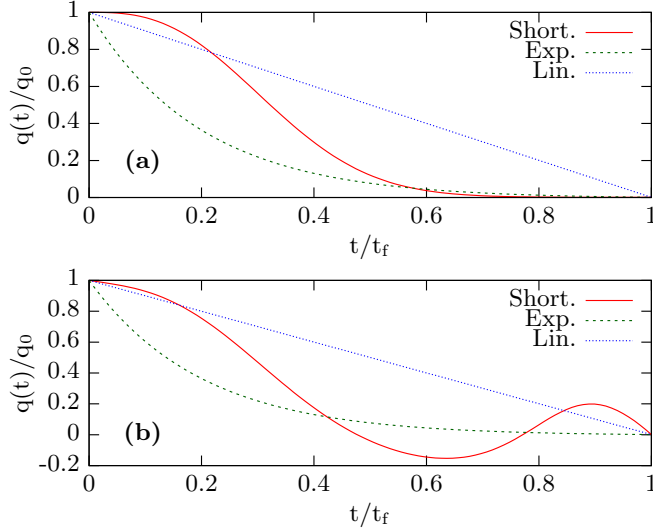


FIG. 3. Comparison between the linear, exponential, and shortcut ramps. In (a) and (b) $U_s/h = 104.13$ Hz, $q_0 = U_s$, and $q_f/q_0 = 10^{-3}$. (a) We consider a slow evolution, with $t_f = 1$ s; (b) a shorter evolution is considered, $t_f = 0.01$ s.

be used to design more constrained protocols depending on the specific needs, e.g., avoiding too large values of $q(t)$.

IV. SHORTCUT TO ADIABATICITY IN THE BEC REGIME

In this section, we consider the performance of our shortcut protocol in the BEC regime. That is, our main goal is to

evolve from the ground state of Eq. (1) for an initial value of $q(t=0) = q_0 = U_s$ to the corresponding ground state for $q(t_f) = q_f$ such that $q_0 > q_f \gg U_s/N^2$. Strictly speaking, the choice $q_0 = U_s$ does not comply with the assumption used to derive the protocol, $q(t) \ll U_s$. The reason the protocol can be extended to this situation is that for short times, $t \lesssim t_f/4$, the protocol produces a very small variation of q , and the dynamics thus remains mostly adiabatic.

To judge the quality of the shortcut protocol we compare it to two other ramp shapes, linear and exponential:

$$q_{\text{lin}}(t) = q_0 - (q_0 - q_f)t/t_f, \quad (15)$$

$$q_{\text{exp}}(t) = (q_0 - q_f) \frac{e^{-\alpha t/t_f} - e^{-\alpha}}{1 - e^{-\alpha}} + q_f.$$

The linear ramp is uniquely determined, and the exponential ramp was found to provide the best results for a decay constant $\alpha = 5$, a value we have used in all the reported results. In Fig. 3 we compare the three ramps considered for a slow evolution [see Fig. 3(a)] and for a faster one [see Fig. 3(b)]. The resulting shortcut protocol is in all cases a smooth function. As shown in the figure, for smaller values of t_f , the protocol has a more pronounced structure, requiring in some cases negative intermediate values of $q(t)$.

We benchmark our shortcut protocol by numerically solving the full time-dependent Schrödinger equation with \hat{H} from Eq. (1) for a particular ramp. We used the mean-squared spin $\langle \hat{S}^2 \rangle$ as a fidelity witness. Note that in the regime we consider in this section, the target final value of q_f is far above the value $\sim U_s/N^2$ below which the ground state reduces to the

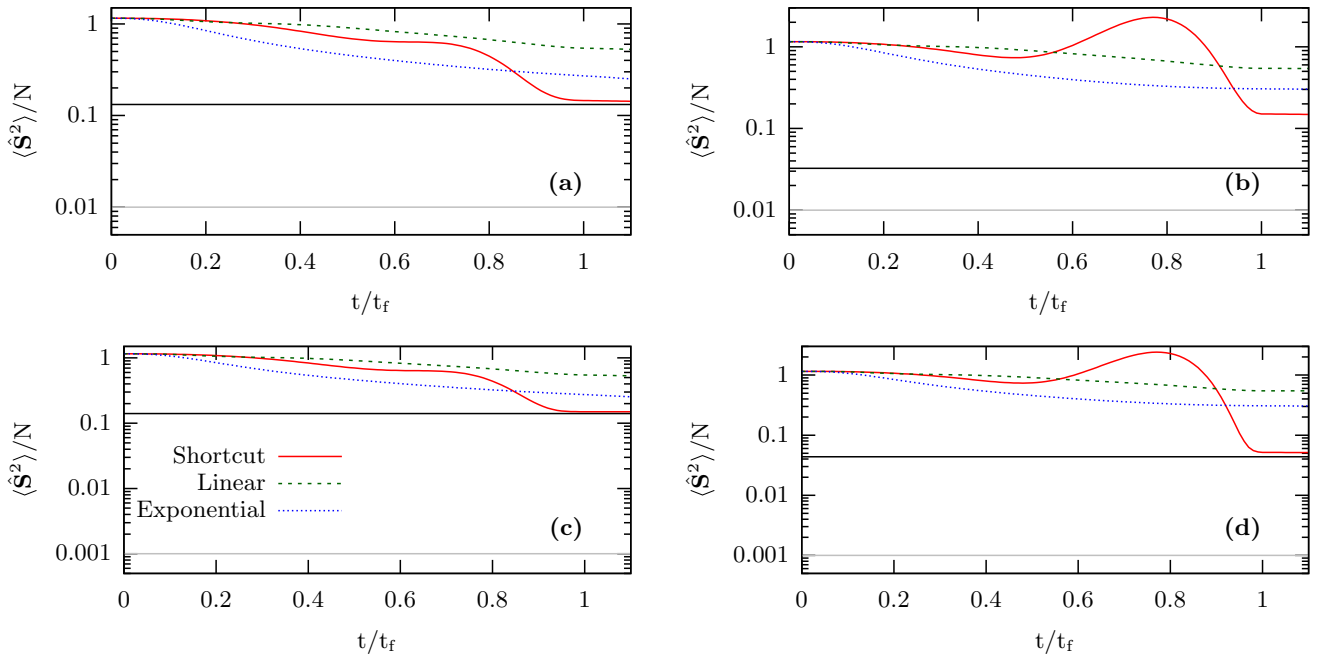


FIG. 4. Mean squared spin $\langle \hat{S}^2 \rangle / N$ as a function of the time computed for systems with $N = 100$ and $N = 1000$ spins evolved following either the shortcut protocol, a linear ramp, or an exponential ramp. All cases describe the evolution of the exact solution of the Schrödinger equation in situations where the evolution is clearly not adiabatic. Only the shortcut protocol brings the system to a state with lower total spin S . In (a)–(d) the initial state corresponds to $N^2 q_0 / U_s = N^2$ and, thus, is deep in the BEC phase (see Fig. 1 in [9]). (a, c) A state at $N^2 q_f / U_s = 0.01 N^2$; (b, d) a final state closer to the fragmented phase $N^2 q_f / U_s = 0.001 N^2$. (a, b) Computed with $N = 100$; (c, d) computed with $N = 1000$. Horizontal black and light-gray solid lines show the level of fluctuations in the ground state for $q = q_f$ and the reference value $\langle \hat{S}^2 \rangle / N = 1/N$, respectively. In all cases, $U_s/h = 104.13$ Hz and $t_f = 0.01$ s.

total spin-singlet state. As a result, the value of $\langle \hat{S}^2 \rangle$ in the ground state corresponding to q_f fulfills $1 \ll \langle \hat{S}^2 \rangle \ll N$.

In Fig. 4 we present the first results, corresponding to two dynamical situations. The first one, shown in Figs. 4(a) and 4(c), goes from $q_0/U_s = 1$ to $q_f/U_s = 0.01$. The second one, shown in Figs. 4(b) and 4(d), goes one order of magnitude smaller, to $q_f/U_s = 0.001$. Also, we compare in the figure two values of N : 100 and 1000. Several features can be observed. In all cases, the shortcut protocol performs clearly better than the other two ramps, while the exponential ramp performs better than the linear ramp. The spin witness $\langle \hat{S}^2 \rangle$ at the final time $t_f = 0.01$ s is substantially lower for the shortcut protocol ($\langle \hat{S}^2 \rangle$ decreases by an order of magnitude from its initial value) and closer to the value expected in the final ground state for larger N . In comparison, the other two protocols are only able to decrease it by at most a factor of 4 in the same time. Moreover, the final value of $\langle \hat{S}^2 \rangle$ decreases with increasing atom number at a fixed t_f . Equivalently, the final fidelities obtained with the shortcut protocol improve as we increase N . This could be expected, as we have obtained our protocol in the large- N limit, thus making the protocol closer to an exact description as N is increased. The results obtained with the exponential and linear ramps are mostly independent of the number of particles.

It is also interesting to see how the wave function evolves in time, going from a state with large $\langle \hat{S}^2 \rangle$, where c_S values are centered around a large S , to a state with small $\langle \hat{S}^2 \rangle$, where the wave function takes substantial values around $S = 0$ or $S = 2$. In Fig. 5 we compare the wave functions at different times

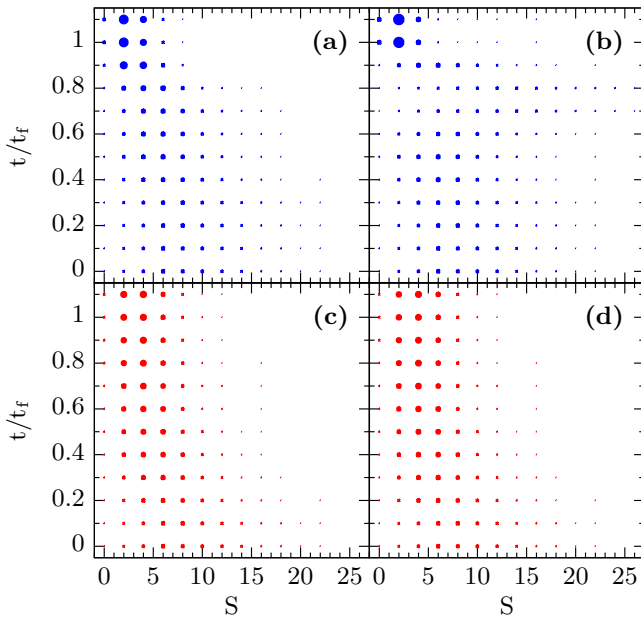


FIG. 5. Time evolution of the wave function. The radii of circles indicate the value of $|c_S|^2$ for each S at each time t/t_f . Blue circles correspond to a system evolved using the shortcut protocol and red circles correspond to a system evolved with an exponential ramp. (a, c) Evolution of a system from $q_0/h = 104.13$ Hz to $q_f = 10^{-2}q_0$ in $t_f = 0.01$ s and (b, d) evolution of a system from $q_0/h = 104.13$ Hz to $q_f = 10^{-3}q_0$ in $t_f = 0.01$ s; this figure can be directly compared to Fig. 4. Since only the even solution is considered, the wave function c_S at odd S is identically 0.

obtained with the shortcut [Figs. 5(a) and 5(b)] and exponential [Figs. 5(c) and 5(d)] protocols. The calculations correspond to the $N = 100$ ones reported in Fig. 4. As is clearly shown in all cases the wave function for the shortcut is much more peaked around $S = 0$ than the exponential one. Also, as expected, the final wave function is more concentrated at smaller values of S as we target final states with smaller q_f . This can be seen comparing Figs. 5(a) and 5(c), computed with $q_f N^2/U_s = 0.01N^2$, with Figs. 5(b) and 5(d), computed with $q_f N^2/U_s = 0.001N^2$. Finally, note that even though the shortcut performs quite well, the final wave function is peaked at $S = 2$ rather than at $S = 0$, which reflects the fact that we are still on the single-BEC side of the crossover reported in Fig. 2(c).

V. SHORTCUT FROM A BEC TO A FRAGMENTED CONDENSATE

In the previous section we have shown the superior performance of the shortcut protocol in comparison with exponential and linear ramps in the BEC regime, $qN^2/U_s \gg 1$. In this section we explore the fragmented condensate domain, that is, QZE ramps going from $q_0N^2/U_s \gg 1$ to $q_fN^2/U_s \lesssim 1$.

In Figs. 6 and 7, we provide an extensive comparison between our shortcut protocol and the linear and exponential ramps. The figures depict the final values of $\langle \hat{S}^2 \rangle$ (Fig. 6) and $\Delta N_0/N$ (Fig. 7). In these figures we consider $N = 500$ atoms, starting from the ground state corresponding to a value of $q_0 = 0.1U_s$. The figures cover a broad range of final target values of q_f , ranging from deep in the BEC sector to well below the transition to the fragmented condensate region, $q_f N^2/U_s \lesssim 1$ (see Fig. 2, upper panel). Results are also reported as a function of the desired final time, t_f . We again take $U_s/h = 104.13$ Hz and final times ranging from 0.001 to 10 s.

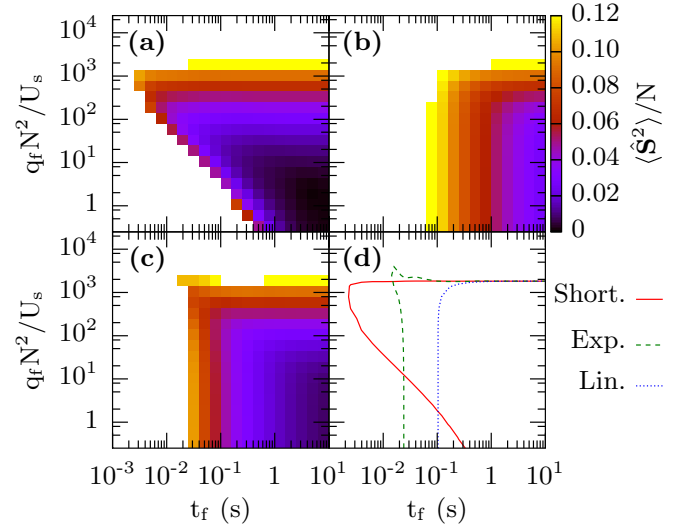


FIG. 6. Value of $\langle \hat{S}^2 \rangle / N$ after the time evolution, i.e., $t = t_f$, for the three protocols considered: (a) shortcut, (b) linear, and (c) exponential. In all cases only the results that give $\langle \hat{S}^2 \rangle / N < 0.12$ are shown. (d) The contour lines corresponding to $\langle \hat{S}^2 \rangle / N = 0.12$. In all cases we have $N = 500$ particles and an initial value of $q_0/h = 0.1 U_s/h = 10.413$ Hz.

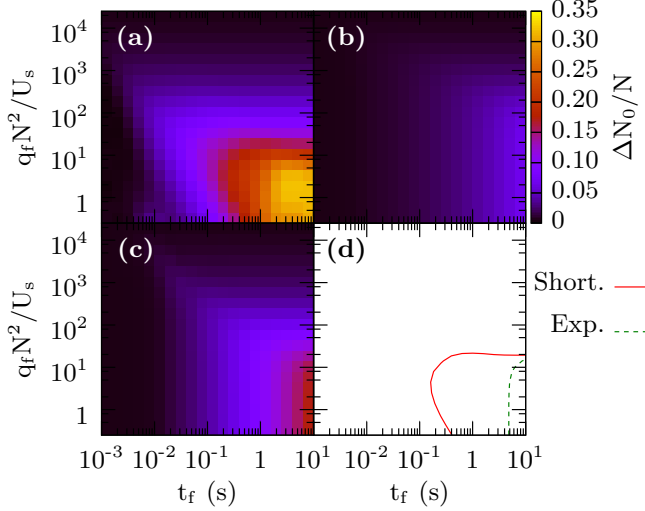


FIG. 7. $\Delta N_0/N$ for the same conditions as in Fig. 6. Results obtained from the three protocols: (a) the shortcut, (b) the linear ramp, and (c) the exponential ramp. (d) The contour lines of the three cases in (a)–(c) for $\Delta N_0/N = 0.15$. All these plots have been realized using a system of $N = 500$ particles and $q_0/h = 0.1 U_s/h = 10.413$ Hz.

As found previously, the shortcut protocol performs better than the exponential and linear ramps in the BEC region, as can be seen by looking at the $q_f N^2/U_s \gtrsim 1$ region in the three figures. For instance in the region in the $(q_f N^2/U_s, t_f)$ map, where small final values of $\langle \hat{S}^2 \rangle$ are larger for the shortcut protocol. The exponential produces also relatively low values, with a result mostly independent of the value of q_f , while the linear ramp fails to produce small final values, unless $t_f \simeq 10$ s.

In situations in which the target final state is clearly in the fragmented domain, $q_f N^2/U_s \simeq 1$, the only method that produces sizable fragmentation, as measured by $\Delta N_0/N \gtrsim 0.15$, is the shortcut protocol (see Fig. 7). The exponential ramp requires times almost two orders of magnitude larger to obtain the same level of fragmentation in the system. In line with the latter, lower final values of $\langle \hat{S}^2 \rangle$ are obtained for the shortcut protocol in those cases in which the fragmentation is closer to the singlet value $\Delta N_0/N \simeq \sqrt{4/45} = 0.298$ [9]. For the parameters considered here, a shortcut ramp performed in $t_f \sim 1$ s is able to produce a state very close to the ground state, for $N = 500$. Note that, using the notations and assumptions from Sec. II C, the chosen value of $U_s/h \approx 10$ Hz is achieved in a trap of frequency $\omega/(2\pi) \approx 300$ Hz for $N = 500$. The corresponding three-body lifetime is $\Gamma_3 \approx 1300$ s $^{-1}$, or $N\Gamma_3 t_f \approx 0.4$: less than a single three-body loss event (on average) during the entire shortcut protocol. Losses should not be a concern for $N \sim 500$.

VI. COMPARISON WITH CURRENT EXPERIMENTAL SETUPS

We have been using, throughout this paper, parameters taken from realistic proposals, most of them from [9]. In this section, we explore different parameters taken from other experimental setups. Some experiments [18] have been done

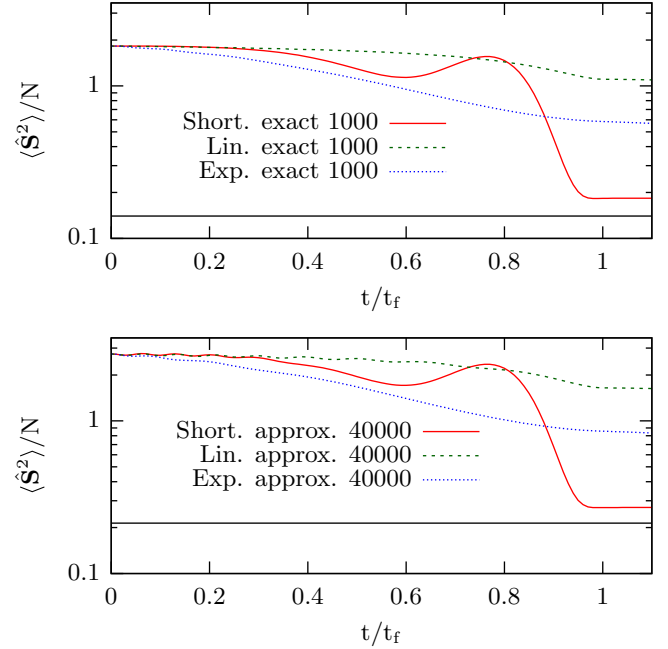


FIG. 8. $\langle \hat{S}^2 \rangle/N$ as a function of time computed for systems evolved following the shortcut protocol, a linear ramp, or an exponential ramp. We compare a system of $N = 1000$ spins (exact solution) and a system of $N = 40000$ spins (approximate solution). The system is evolved from a state with $q_0/h = 10 U_s/h = 71$ Hz to $q_f = 10^{-3} q_0$ in $t_f = 0.1$ s. The shortcut protocol also works for this set of parameters, although it is, in principle, valid only for $q(t) \ll U_s$, in the sense that it provides a clear gain over simpler exponential or linear ramps. For $N = 1000$ and $N = 40000$ the corresponding values of $N^2 q_f/U_s$ are 10^4 and 16×10^6 . The solid black line is the ground-state value for $q = q_f$.

recently with ^{87}Rb Bose condensates composed of $N = 40000$ atoms with $U_s/h = 7.1$ Hz and a $q(t)$ around $10U_s$. Taking these parameters, we have calculated the evolution of a system with $N = 1000$ particles and $U_s/h = 7.1$ Hz to check whether the shortcut protocol still gives good results under these experimental conditions. Results have also been obtained for a system with $N = 40000$ spins using the shortcut protocol for the approximate Hamiltonian in Eq. (7). In Fig. 8 both results are shown for comparison.

$\langle \hat{S}^2 \rangle$, shown in Fig. 8, has been computed for these two systems, and although the initial values of $q(t)$ are larger than U_s , the shortcut protocol still drives the system to the ground state (or close) and improves the performance of the other two ramps. Although the shortcut protocol is, in principle, valid only for $q(t) \ll U_s$, this and other calculations (where we have driven a system from different values of q_0 , all between 10 and 1000 times larger than U_s , to q_f above and below U_s) show that the protocol can be successfully applied for larger q_0 values.

VII. SUMMARY AND CONCLUSIONS

We have presented a method to prepare a spin-1 BEC into a many-body spin-singlet state by making use of an approximate protocol to shortcut the adiabatic following in the many-body system. The protocol consists in specific functions $q(t)$ which

are constructed such that the time evolution of the system brings the many-body state from the ground state for $q_0 \equiv q(t=0)$ to the ground state for $q_f \equiv q(t=t_f)$. The main aim is to produce the very fragmented ground state of the spinor system in the absence of a quadratic magnetic field, starting from a condensate in the $m=0$ manifold in a regime dominated by the quadratic Zeeman term. The performance of the shortcut protocol has been compared to both a linear and an exponential ramp of the parameter q .

Even though the protocol is only approximate, it is shown to provide a much better performance than the exponential and linear ones in almost all situations. In the BEC case, that is, for $qN^2/U_s \gg 1$, the method works almost perfectly for time intervals of the order of $1/U_s$ and larger. The method also works better for cases in which the BEC-fragmented transition is targeted. In particular, it works with an accuracy similar to that of the exponential ramp up to times one order of magnitude smaller. To quantify the performance we have computed the achieved final value of $\langle \hat{S}^2 \rangle$ and the value of $\Delta N_0/N$.

We have obtained results for systems of different sizes and final and initial setups and we have seen that the protocol achieves better results for larger systems. Results have also been obtained from approximate solutions of the Schrödinger equation [using Eqs. (7) and (8)]. Based on these results we have been able to extrapolate the method to larger systems and find that, with this protocol, a many-body spin-singlet state can be obtained for many different system sizes. We have also shown the success of our method when applied to systems prepared with parameters taken from current experimental setups. We believe that our method for preparing a BEC in a singlet state with short times is experimentally realizable and efficient. Further improvements to the shortcut protocol profiting from the available freedom inherent in the presented procedure will be the object of forthcoming investigations.

ACKNOWLEDGMENTS

We acknowledge stimulating discussions with members of the Bose-Einstein condensates group at LKB, in particular, with Bertrand Evrard and Jean Dalibard and with Tommaso Roscilde. This work was partially supported by DARPA (Optical Lattice Emulator Grant). We acknowledge financial support from the Spanish MINECO (FIS2014-54672-P), Generalitat de Catalunya Grant No. 2014SGR401, and Maria de Maeztu Grant No. MDM-2014-0369. L.D.S. acknowledges support from the EU (Marie Curie IEF Grant No. 236240), and T.Z. from the Hamburg Center for Ultrafast Imaging. B.J.-D. was supported by the Ramón y Cajal MINECO program.

APPENDIX A: ZEEMAN ENERGY IN SPINOR CONDENSATES

For a single alkali atom, the Zeeman energy in a weak applied magnetic field B is given by the expansion of the exact Breit-Rabi formula in powers of $\mu_B B / \hbar \omega_{\text{hf}} \ll 1$. For $F=1$ atoms (^{87}Rb or ^{23}Na), one has

$$\hat{H}_{\text{mag}} = -p\hat{S}_z + q(\hat{S}_z^2 - 4), \quad (\text{A1})$$

with \hat{S}_z the z projection of the spin of the atom. The quantities $p = \mu_B B/2$ and $q = (\mu_B B)^2 / (4\hbar\omega_{\text{hf}})$ are the linear and quadratic Zeeman shifts, respectively, $\hbar\omega_{\text{hf}}$ is the hyperfine energy splitting in the electronic ground state, and μ_B is the Bohr magneton. [For sodium atoms, $\omega_{\text{hf}}/(2\pi) \approx 1.772$ GHz, $\mu_B/2 \approx \hbar \times 0.696$ MHz/G, and $q/\hbar B^2 \approx 277$ Hz/G².] For many atoms, we have, in second-quantized notation,

$$\hat{H}_{\text{Zeeman}} = -p\hat{S}_z - q(\hat{N}_0 + 3N). \quad (\text{A2})$$

Importantly, in many experiments the linear Zeeman shift αp is irrelevant. The reason is that binary s -wave collisions that are responsible for establishing kinetic equilibrium enjoy spin rotational symmetry and, therefore, cannot change the value of the magnetization [11]: For short enough time scales \hat{S}_z is effectively a conserved quantity. For long times, there are decay mechanisms that act as relaxation channels for \hat{S}_z , for instance, inelastic losses such as dipolar relaxation or three-body collisions. These processes typically degrade the spin correlations as well (see discussion in Sec. II C), and we assume that they occur at time scales much longer than the dynamics studied throughout this paper. We do not expect our results to be substantially modified by a slow and weak relaxation of the magnetization during the ramp of q .

APPENDIX B: EIGENSTATES OF THE HAMILTONIAN IN THE $|N, S, M\rangle$ BASIS

The Hamiltonian in Eq. (1) is diagonalized by the total spin eigenstates $|N, S, M\rangle$, where S is the total spin and M the total projection of S in the z -axis direction. A general state ϕ_M is written as, $|\phi_M\rangle = \sum_{S=|M|}^N c_S |N, S, M\rangle$. The construction of the angular momentum eigenstates is not trivial, and these are built as [3–6,9]

$$|N, S, M\rangle = \frac{1}{\mathcal{Z}(N, S, M)^{1/2}} (\hat{S}_-)^P (\hat{A}^\dagger)^Q (\hat{a}_{+1}^\dagger)^S |\text{vac}\rangle, \quad (\text{B1})$$

where $P = S - M$, $2Q = N - S$, \hat{a}_i^\dagger and \hat{a}_i are the creation and annihilation operators of state i , respectively, $\hat{S}_- = \sqrt{2}(\hat{a}_{-1}^\dagger \hat{a}_0 + \hat{a}_0^\dagger \hat{a}_{+1})$ is the lowering total spin operator, and $\hat{A}^\dagger = (\hat{a}_0^\dagger)^2 - 2\hat{a}_{+1}^\dagger \hat{a}_{-1}^\dagger$ is the singlet creation operator.

The expression of these states involves three operators. The first one, \hat{a}_{+1}^\dagger , is the creation operator of a spin-1 particle with $m = +1$. This operator acting S times over the vacuum leads to the many-particle state $\propto |S, S, S\rangle$. The acting operators \hat{A}^\dagger and \hat{S}_- commute with the total spin momentum operator and therefore do not modify S . The singlet creator operator creates pairs with total spin 0, so it only changes the number of particles. Then Q repeated actions of this operator add singlet pairs until the state $\propto |N, S, S\rangle$ is obtained. Finally, the lowering angular momentum operator S_- acts $P = S - M$ times without affecting N or S , leading to the final state $\propto |N, S, M\rangle$. The normalization factor is obtained after tedious calculations:

$$\mathcal{Z}(N, S, M) = S! \frac{(N-S)!(N+S+1)!}{(2S+1)!} \frac{(S-M)!(2S)!}{(S+M)!}. \quad (\text{B2})$$

The complete Hamiltonian in Eq. (1) can be computed in the N, S, M basis. The interaction term is diagonal, but the

operator $\hat{N}_0 = \hat{a}_0^\dagger \hat{a}_0$ has matrix elements between states with S and states $S \pm 2$. The total Hamiltonian is thus tridiagonal and therefore easy to solve numerically. The action of \hat{N}_0 is explicitly given by [9]

$$\begin{aligned} & q\hat{N}_0|N S M\rangle \\ &= q\sqrt{A_-(N, S+2, M)A_+(N, S, M)}|N S+2 M\rangle \\ &+ q\sqrt{A_+(N, S-2, M)A_-(N, S, M)}|N S-2 M\rangle \\ &+ q[A_-(N, S, M) + A_+(N, S, M)]|N S M\rangle, \end{aligned} \quad (\text{B3})$$

where

$$\begin{aligned} A_+(N, S, M) &= \frac{(S+M+1)(S-M+1)(N-S)}{(2S+1)(2S+3)}, \\ A_-(N, S, M) &= \frac{(S+M)(S-M)(N+S+1)}{(2S+1)(2S-1)}. \end{aligned} \quad (\text{B4})$$

The resulting Hamiltonian, given also in Eq. (4), reads

$$h_{S,S+2} c_{S+2} + h_{S,S-2} c_{S-2} + h_{S,S} c_S = E c_S, \quad (\text{B5})$$

with

$$\begin{aligned} h_{S,S+2} &= -q\sqrt{(N+S+3)(N-S)} \\ &\quad \times \frac{(S+1)(S+2)}{(2S+3)\sqrt{(2S+1)(2S+5)}}, \\ h_{S,S-2} &= -q\sqrt{(N+S+1)(N-S+2)} \\ &\quad \times \frac{S(S-1)}{(2S-1)\sqrt{(2S+1)(2S-3)}}, \\ h_{S,S} &= \frac{U_s}{2N} S(S+1) \\ &\quad - q \left[\frac{S^2(N+S+1)}{(2S-1)(2S+1)} + \frac{(S+1)^2(N-S)}{(2S+1)(2S+3)} \right]. \end{aligned} \quad (\text{B6})$$

APPENDIX C: CONTINUUM APPROXIMATION OF THE HAMILTONIAN

A continuum approximation of Eq. (4) can be obtained by considering $1 \ll S \ll N$. The wave function c_S can, thus, be approximated by a continuous function $c(x)$, where $x \equiv S/N$ and varies from 0 to 1. Then $\epsilon = 2/N$ can be taken as a small parameter and a Taylor expansion can be made:

$$c_{S\pm 2} = c(x) \pm \epsilon c'(x) + \frac{\epsilon^2}{2} c''(x) + O(\epsilon^3). \quad (\text{C1})$$

Upon substituting this expression into Eq. (4) the following continuum Schrödinger equation is obtained:

$$\alpha(x)c''(x) + \beta(x)c'(x) + [\gamma(x) - E]c(x) = 0, \quad (\text{C2})$$

where

$$\begin{aligned} \alpha(x) &= \frac{\epsilon^2}{2}(h_{S,S+2} + h_{S,S-2}), \\ \beta(x) &= \epsilon(h_{S,S+2} - h_{S,S-2}), \\ \gamma(x) &= h_{S,S} + h_{S,S+2} + h_{S,S-2}. \end{aligned} \quad (\text{C3})$$

Taking into account that $1 \ll S \ll N$, we can set the order until the one we want to approximate. Performing a Taylor expansion in S/N , $1/S$, and $1/N$ and substituting the resulting expressions in Eqs. (C3), one finds

$$\begin{aligned} \alpha(x) &\approx -\frac{q}{N} \left(1 - \frac{x^2}{2} + \frac{3}{2N} \right), \\ \beta(x) &\approx \frac{-q}{4N^2 x^2} \left(1 - \frac{x^2}{2} + \frac{3}{2N} \right), \\ \gamma(x) &\approx \frac{N}{2} U_s x^2 - qN \left(1 - \frac{x^2}{4} + \frac{1}{2N} + \frac{1}{8N^2 x^2} \right). \end{aligned} \quad (\text{C4})$$

Keeping terms to leading order in $1/N, x$ we arrive at the Schrödinger-like equation, (7).

-
- [1] E. J. Mueller, T. L. Ho, M. Ueda, and G. Baym, *Phys. Rev. A* **74**, 033612 (2006).
- [2] P. Nozières, in *Bose-Einstein Condensation*, edited by A. Griffin, D. W. Snoke, and S. Stringari (Cambridge University Press, Cambridge, UK, 1995).
- [3] C. K. Law, H. Pu, and N. P. Bigelow, *Phys. Rev. Lett.* **81**, 5257 (1998).
- [4] T.-L. Ho and S. K. Yip, *Phys. Rev. Lett.* **84**, 4031 (2000).
- [5] M. Koashi and M. Ueda, *Phys. Rev. Lett.* **84**, 1066 (2000).
- [6] Y. Castin and C. Herzog, *CRAS Paris* **2**(4), 419 (2001).
- [7] F. Zhou, *Int. J. Mod. Phys. B* **17**, 2643 (2003).
- [8] R. Barnett, J. D. Sau, and S. Das Sarma, *Phys. Rev. A* **82**, 031602 (2010).
- [9] L. De Sarlo, L. Shao, V. Corre, T. Zibold, D. Jacob, J. Dalibard, and F. Gerbier, *New J. Phys.* **15**, 113039 (2013).
- [10] V. Corre, T. Zibold, C. Frapolli, L. Shao, J. Dalibard, and F. Gerbier, *Europhys. Lett.* **110**, 26001 (2015).
- [11] D. M. Stamper-Kurn and M. Ueda, *Rev. Mod. Phys.* **85**, 1191 (2013).
- [12] E. Torrontegui, S. Ibañez, S. Martínez-Garaot, M. Modugno, A. del Campo, D. Guéry-Odelin, A. Ruschhaupt, X. Chen, and J. G. Muga, *Adv. At. Mol. Opt. Phys.* **62**, 117 (2013).
- [13] S. An, D. Lv, A. del Campo, and K. Kim, *Nat. Commun.* **7**, 12999 (2016).
- [14] X. Chen, A. Ruschhaupt, S. Schmidt, A. del Campo, D. Guéry-Odelin, and J. G. Muga, *Phys. Rev. Lett.* **104**, 063002 (2010).
- [15] B. Juliá-Díaz, E. Torrontegui, J. Martorell, J. G. Muga, and A. Polls, *Phys. Rev. A* **86**, 063623 (2012).
- [16] A. Yuste, B. Juliá-Díaz, E. Torrontegui, J. Martorell, J. G. Muga, and A. Polls, *Phys. Rev. A* **88**, 043647 (2013).
- [17] S. Campbell, G. De Chiara, M. Paternostro, G. M. Palma, and R. Fazio, *Phys. Rev. Lett.* **114**, 177206 (2015).
- [18] T. M. Hoang, M. Anquez, B. A. Robbins, X. Y. Yang, B. J. Land, C. D. Hamley, and M. S. Chapman, *Nat. Commun.* **7**, 11233 (2016).
- [19] F. Gerbier, A. Widera, S. Fölling, O. Mandel, and I. Bloch, *Phys. Rev. A* **73**, 041602(R) (2006).
- [20] S. Knoop, T. Schuster, R. Scelle, A. Trautmann, J. Appmeier, M. K. Oberthaler, E. Tiesinga, and E. Tiemann, *Phys. Rev. A* **83**, 042704 (2011).
- [21] A. Görlitz, T. L. Gustavson, A. E. Leanhardt, R. Löw, A. P. Chikkatur, S. Gupta, S. Inouye, D. E. Pritchard, and W. Ketterle, *Phys. Rev. Lett.* **90**, 090401 (2003).